Journal of Sound and Vibration 424 (2018) 352–364

Contents lists available at ScienceDirect

Journal of Sound and Vibration

journal homepage: www.elsevier.com/locate/jsvi

Reducing mechanical cross-coupling in phased array transducers using stop band material as backing

J. Henneberg [a,c,*], A. Gerlach [a], H. Storck [a], H. Cebulla [b], S. Marburg [c]

[a] Robert Bosch GmbH, Robert-Bosch-Campus 1, 71272 Renningen, Germany
[b] Technical University Chemnitz, Professorship for Textile Technologies, Reichenhainer Str. 31/33, 09126 Chemnitz, Germany
[c] Technical University of Munich, Chair of Vibroacoustics of Vehicles and Machines, Boltzmann Str. 15, 85748 Garching, Germany

ARTICLE INFO

Article history:
Received 21 September 2017
Revised 31 January 2018
Accepted 15 March 2018
Available online 30 March 2018

Dedicated to Professor Franz Holzweißig on the occasion of his 90th birthday.

Keywords:
Local resonator
Tuned resonator
Stop band material
Acoustic metamaterial
Phased array transducer
Cross-coupling

ABSTRACT

Phased array transducers are widely used for acoustic imaging and surround sensing applications. A major design challenge is the achievement of low mechanical cross-coupling between the single transducer elements. Cross-coupling induces a loss of imaging resolution. In this work, the mechanical cross-coupling between acoustic transducers is investigated for a generic model. The model contains a common backing with two bending elements bonded on top. The dimensions of the backing are small; thus, wave reflections on the backing edges have to be considered. This is different to other researches. The operating frequency in the generic model is set to a low kHz range. Low operating frequencies are typical for surround sensing applications. The influence of the backing on cross-coupling is investigated numerically. In order to reduce mechanical cross-coupling a stop band material is designed. It is shown numerically that a reduction in mechanical cross-coupling can be achieved by using stop band material as backing. The effect is validated with experimental testing.

1. Introduction

Phased array structures of acoustic transducers are used for acoustic imaging in medical applications and for nondestructive testing. Furthermore, there are applications for 3D surround sensing. Depending on the field of use, the typical operating frequency varies in a range from lower kHz for surround sensing [1,2] up to several MHz for nondestructive testing [3] and medical applications [4]. One of the characteristic properties of these structures is the cross-coupling between single transducers. It mainly describes the undesired behavior that array elements are not working independently [5]. In several studies it has been shown that cross-coupling influences the performance of a phased array by changing its beam pattern and resulting in a loss of resolution [5–8]. In Ref. [5] a quantitative theory for cross-coupling in ultrasonic transducer arrays is presented. Surface waves in the backing and in the load medium in front of the transducers are indicated as reason for cross-coupling. This theory assumes a series of uniformly distributed, unbacked transducer elements. The cross-coupling is caused by interaction through a semi-infinite substrate, the solid load medium. In Ref. [9] a basic model and influence of cross-coupling with focus on cross-coupling included signals is given. Lamb wave A0 mode has been identified as the responsive effect for cross-coupling in a CMUT-array (capacitive micromachined ultrasonic transducer) with first order resonance at 2.3 MHz [10]. An air-coupled, low frequency phased array is presented in the studies [11]. The ultrasonic transducers are realized with piezoelectric crystals. As

* Corresponding author. Robert Bosch GmbH, Robert-Bosch-Campus 1, 71272 Renningen, Germany.
E-mail addresses: Johannes.Henneberg@de.bosch.com, johannes.henneberg@tum.de (J. Henneberg).

https://doi.org/10.1016/j.jsv.2018.03.021

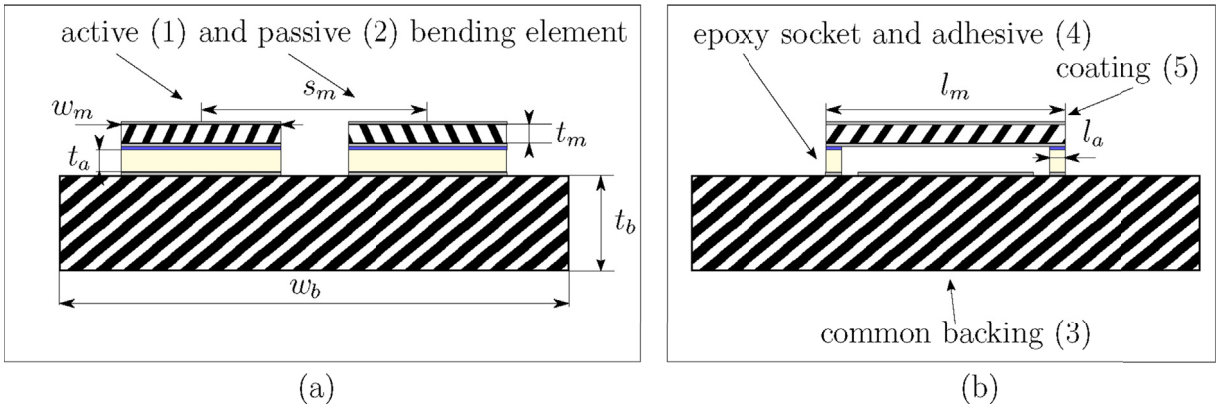

Fig. 1. Investigated generic model with 2 bending elements on a common backing. (a) frontal view, (b) side view.

the used setup with piezoelectric elements and foam as spacer does not cause high cross-coupling, it is not further investigated. In Refs. [12,13] cross-coupling is investigated in a finite element model of a linear, piezoceramic based phased array transducer.

In this study, we investigate the cross-coupling of a generic transducer array model with a low operating frequency at 5.2 kHz. We focus especially on mechanical cross-coupling caused by the common backing without extra lossy regions. The realization of extra lossy regions between every transducer element requires high effort in real structures. Thus, a design without extra lossy regions is desired. Cross-coupling caused by the common backing is the dominating effect in air-coupled transducer arrays. The dimensions of the backing are small, thus wave reflections on the edges of the backing have to be taken into account in simulations of the whole model. This is different to other researches. The design of the backing is a major challenge in phased array transducers with low operating frequency. To overcome this problem, we show that stop band materials can be used to reduce mechanical cross-coupling caused by common backing in phased array structures. Stop band materials, also known as acoustic metamaterials, consist out of periodic structure with particular dynamic behavior in a certain frequency range. Hence it is clarified that stop band material describes a structural but not a material behavior.

In recent years, stop band materials received a growing attention. In analogy to photonic crystals, Ref [14] presents a study with experimental investigation on sonic crystals to design band gap behavior. Therefore, rigid spheres of lead were coated with rubber and placed in an epoxy plate. Stop band materials can decrease acoustical [15] as well as vibrational [16] responses of components in certain frequency bands. Thus, bragg scattering and local resonant structures can be used. As Bragg scattering is based on destructive interference effects [17], a periodic lattice is required. In contrary, resonant stop bands can be achieved by ordered and disordered structures. This is shown for an electromagnetic metamaterial in Ref. [18] and for an acoustic metamaterial in Ref. [19]. However, the scale of the stop band material should be smaller than the wavelength to be attenuated. In this study, ordered periodic resonant structures are investigated. In Ref. [15], it is shown that resonant stop bands have a good prospect for low frequency stop bands. In Ref. [20], it is shown that propagation of flexural waves in thin plates can be attenuated by locally attached spring-mass resonators. In Ref. [21], a possible application for microfabricated phononic crystal waveguides is named but not investigated in detail. The intention is to route and bend acoustic signals from large electro-acoustic transducers to be emitted and detected through small apertures. By this, the resolution of phased array structures can be increased.

Initially we focus on a generic model to investigate the relation between dynamical behavior of the backing and cross-coupling. In finite element simulation, we analyze the dependence of cross-coupling on the backing thickness. Afterwards, we investigate an extended model with stop band material as backing. In simulation as well as in experimental testing, the effect of locally resonant structures with regard to mechanical cross-coupling is shown. Finally, a conclusion is drawn.

2. Cross-coupling in phased array transducer

In this section we give an overview of the investigated generic model. The calculation of cross-coupling is defined and its mechanism is shown for the generic model.

2.1. Generic model setup

In analogy to CMUT-arrays, a generic model is set up with two bending elements bonded on a square, common backing. Each bending element forms an electrode of a capacitive transducer. The counter-electrodes are realized on the common backing. To achieve electrical conductivity, the bending elements and the backing are coated with aluminum (5). The cross-section of this generic model is shown in Fig. 1. The two bending elements (1 + 2) are made of carbon fiber reinforced plastic (CFRP) coated with aluminum. They are bonded with a cyanoacrylate adhesive to epoxy sockets (4) on a common epoxy backing (3).

The dimensions are given in Table 1. This setup is comparable with the setup up given in Ref. [10]. The main differences are

Table 1
Dimensions of the generic setup to investigate the influence of backing thickness on cross-coupling in phased array transducers.

Parameter		Symbol	Value	Parameter		Symbol	Value
Backing	thickness	t_b	1.0–16.0 mm	Bending element	thickness	t_m	0.5 mm
	width	w_b	70.0 mm		width	w_m	6.0 mm
Epoxy socket	thickness	t_a	30 µm		spacing	s_m	24.0 mm
	length	l_a	4.6 mm		length	l_m	30.0 mm

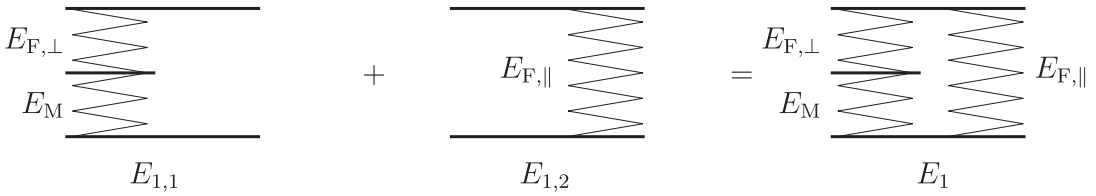

Fig. 2. Rheological model of CFRP along direction 1 according to [22].

- the ratio between bending element thickness and backing thickness,
- the rectangular shape of the bending element,
- the first resonance frequency is much lower and
- there is no extra lossy region.

These differences lead to a different dynamic behavior. Especially the missing extra lossy region causes wave reflection on the edges of the backing. Taking this into account is important to overcome design challenges for the backing in air-coupled phased array transducers with low operating frequency.

All investigations are based on this generic model. The operating frequency in this generic model is set to approximately 5 kHz which is much lower than in surround sensing applications. This finally relieve the specimen preparation for experimental testing. The results can be transferred to higher frequency ranges easily.

2.2. Material model

Composite materials such as CFRP require higher effort to be simulated in a proper way. They consist at least of two different materials and show non-isotropic behavior. Homogenization is a common approach to model these material. By this, the material behavior is described with surrogate parameters which represent the global behavior of the homogenized material. We apply an orthotropic material model which is developed in Ref. [22]. The rheological model assumes a series and parallel circuit of fiber (index_F) and matrix (index_M) material properties. This model is given in Fig. 2.

Eq. (1) describes the behavior as a series circuit of properties of the matrix material and the fiber perpendicular to its axis ($\perp$). $\Phi_{1,1}$ denotes the fiber volume ratio of the fibers perpendicular to its axis within the series circuit, see Fig. 2 $E_{1,1}$. The nonuniform strain in the matrix is considered by Halpin-Tsai method with the semi-empirical factor β [23,24]. Furthermore Eq. (2) describes the material properties of the fiber along its axis ($\parallel$). The ondulation of woven fabric is taken into account by $\eta \in [0, 1]$ which lowers the Young's modulus due to the anisotropic material properties of carbon fibers.

$$E_{1,1} = \frac{\beta \cdot E_M \cdot E_{F,\perp}}{\Phi_{1,1} \cdot \beta \cdot E_M + (1 - \Phi_{1,1}) \cdot E_{F,\perp}} \tag{1}$$

$$E_{1,2} = \eta \cdot E_{F,\parallel} \tag{2}$$

The theory assumes a balanced woven fabric. Thus, the resulting Young's modulus for direction 1 is calculated as given in Eq. (3), where Φ denotes the overall fiber volume ratio of the composite.

$$E_1 = \frac{\Phi}{2} \cdot E_{1,2} + (1 - \frac{\Phi}{2}) \cdot E_{1,1} \tag{3}$$

Young's modulus, shear modulus and Poisson's ratio are calculated for each direction in a similar way as shown above. The entire description of the applied micro-mechanical material model is extensive. The development of the material model is not within the scope of this study. For this reason, the authors refer to literature eg. Refs. [22–25].

The epoxy backing and socket are modeled with an isotropic material behavior. All resulting material parameters are given in Table 2.

Table 2
Material parameters.

	Epoxy backing	Epoxy socket		CFRP
Density [$\frac{g}{cm^3}$]	1.14	4.3		1.32
Damping [–]	0.035	0.010		0.056
Poisson's ratio [–]	0.33	0.38	$\nu 12$	0.15
			$\nu 13$	0.45
			$\nu 23$	0.45
Young's modulus [MPa]	3500	6094	E1	33424
			E2	33424
			E3	4976
Shear modulus [MPa]			G12	1974
			G13	1715
			G23	1715

2.3. Finite element simulation

In finite element simulation, the structural dynamic behavior is investigated. Therefore, the backing, bending elements and epoxy sockets are modeled. The aluminum layer as well as the cyanoacrylate adhesive are not modeled in the simulation. The thickness of the aluminum layer is only a few hundred nanometers thick. The cyanoacrylate adhesive is also applied as a thin layer. We assume ideal adhesion behavior between the components and negligible influence on the mechanical behavior. The load medium is not part of the model. Thus, no fluid-structure interaction is considered. The excitation for a harmonic analysis is realized by a load applied to one, the active, bending element.

The finite element simulation of the generic model is carried out with the commercial software Simulia Abaqus 6.14. All parts are meshed with twenty-node brick elements with reduced number of integration points (C3D20R). The bending elements are modeled with 0.6 mm average element edge length and 5 layers over thickness. The backing is modeled with 1.0 mm average element edge length and 4 layers over thickness. By this, the guidelines given in Ref. [26] are satisfied. The connections between bending elements, epoxy sockets and backing are modeled with tie constraints by a surface-to-surface formulation. The backing has free-free boundary conditions.

2.4. Cross-coupling definition

In a harmonic analysis and in experiment, a load is applied to the active bending element. The cross-coupling between the active and the passive bending elements is then calculated by

$$P_{\mathrm{n}} = 10 \cdot \lg\left(\frac{\widehat{V}_2}{\widehat{V}_1}\right) \mathrm{dB}\ , \tag{4}$$

where V denotes the integral of squared velocity over the whole area of each bending element. As we assume uniformly distributed mass for the bending elements, V represents a kinetic energy equivalent value. To calculate the cross-coupling between the bending elements, the peak at resonance frequency f_{r_n} of each bending element n is used with $\widehat{V}_n = V(f_{r_n})$. It follows that $\widehat{V}_n$ appears at different frequencies for each bending element. Fig. 3 shows a schematic drawing of velocity spectra of the bending elements. In simulation, $\widehat{V}_n$ appears almost at the same frequency due to ideal conditions in setup accuracy. This is different from real setups, where small differences during the preparation process can change the resonance frequency of each bending element. Thus, a comparable and appropriate validation of cross-coupling in the system can be achieved with $\widehat{V}_n = V(f_{r_n})$ in simulation as well as in experimental tests.

2.5. Cross-coupling dependence on backing

Firstly, the influence of the backing thickness on the cross-coupling is investigated in finite element simulation. The first resonance frequency of the bending elements of the investigated generic model is between 4.9 kHz and 5.2 kHz depending on the backing thickness. The interval to search for $\widehat{V}_n$ is set from 4.5 kHz to 5.6 kHz. Fig. 4 shows that the cross-coupling is highly influenced by the backing thickness. A thicker backing, implying higher stiffness, leads to less cross-coupling. Especially in a range between 2 mm to 6 mm and 9 mm–13 mm, this is not applicable. This is due to the particular dynamic behavior of the backing.

The modes of the system are not well separated. Hence, cross-coupling strongly depends on the particular dynamic behavior of the backing. We want to demonstrate this on the example of two different configurations of the backing thickness, $t_{\mathrm{b}} = 3.0$ mm and $t_{\mathrm{b}} = 4.0$ mm. Fig. 5 (a) shows the mode shapes and the associated eigenfrequencies of the system with $t_{\mathrm{b}} = 3.0$ mm in the range of interest. In the first mode shape, the bending elements move with the opposite phase (out-of-phase). In the second mode shape they move with the same phase (in-phase). The difference in eigenfrequency between in-phase and out-of-phase modes is $\Delta f = 208$ Hz. In comparison, Fig. 5 (b) shows the modes of the system with $t_{\mathrm{b}} = 4.0$ mm. In this case, the

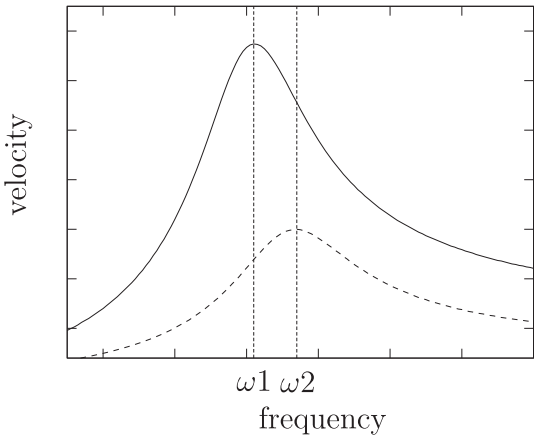

Fig. 3. Scheme of velocity spectra to calculated cross-coupling P_{n}. Frequency of resonance can vary between active (—) and passive bending (- -) element.

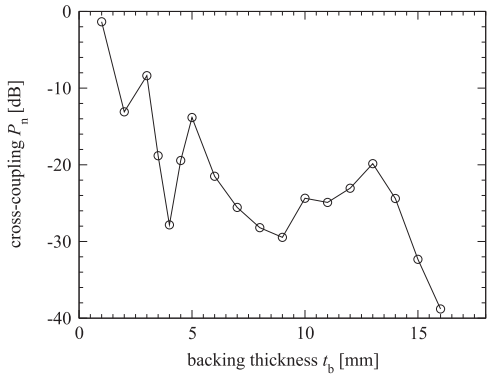

Fig. 4. Cross-coupling P_{n} dependence on backing thickness t_b.

difference in eigenfrequency between the in-phase and out-of-phase modes is only $\Delta f = 20$ Hz. Weak cross-coupling can be attributed to the small difference in eigenfrequency of the in-phase and out-of-phase modes. Similar relations between cross-coupling and difference in eigenfrequency are found in Ref. [27]. Thus, the behavior of weak mechanical cross-coupling caused by a common backing could be interpreted as low transfer mobility between active and passive bending element, caused by strong cancellation between the in-phase and out-of-phase mode. Meanwhile, the influence on the point mobility is negligible. The cancellation effect also depends on the damping of the system. If a system has a certain difference in eigenfrequency Δf between the in-phase and out-of-phase modes, higher damping causes weaker cross-coupling. This can be explained by a higher bandwidth of the peak in the harmonic analysis of in-phase and out-of-phase modal contributions. Thus, the magnitudes of the modal contributions for a certain frequency are more similar than in cases of lower damping. As the phase difference between the modes remains 180°, the cancellation effect is higher in systems with higher damping.

Fig. 6 shows the dependence of cross-coupling P_{n} on the difference in eigenfrequency Δf between the in-phase and out-of-phase modes. The results are calculated in the generic model with the same data as before. The backing thickness t_{b} is varied again in the range from 1 mm to 16 mm. With growing difference in eigenfrequency Δf, the cross-coupling P_n raises.

An outlier can be found for $\Delta f = 12.3$ Hz with cross-coupling of $P_n = -19.4$ dB. This point belongs to the generic model with $t_b = 4.5$ mm. In this case, a weakness of the previous presented method to calculate cross-coupling emerge. In some systems with weak cross-coupling (< -25 dB) nearby modes, dominated by the particular dynamic behavior of the backing, are excited quite strong. Thus, the amplitude $\widehat{V}_2$ is located at a different frequency. By this, a motion of the whole backing is analyzed rather than cross-coupling. An even better result can be achieved by reducing the interval of searching for $\widehat{V}_2$ in this system. To keep the calculation of cross-coupling P_n comprehensible, the authors decide to not change the range of searching for $\widehat{V}_2$ for this system.

Based on the results presented in Fig. 6, it is possible to evaluate the cross-coupling qualitatively in different phased array systems with comparable damping by a modal analysis. The objective to minimize is the difference in eigenfrequency Δf between the in-phase and the out-of-phase modes. This is an advantage for design optimization of phased array structures because a modal analysis requires less computational effort than a harmonic analysis over a broad frequency band.

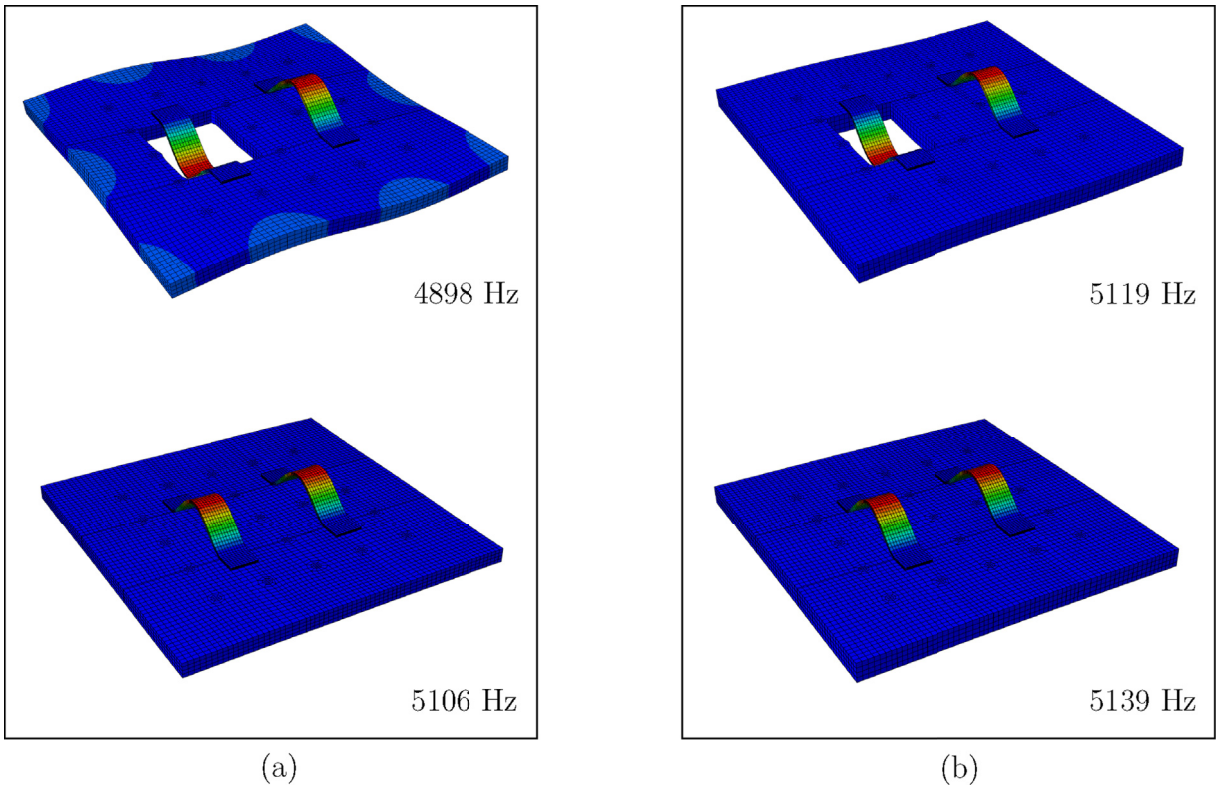

Fig. 5. Modes of interest with backing thickness (a) $t_b = 3.0$ mm and (b) $t_b = 4.0$ mm. Note: For a better visibility, some elements of the backing are not shown in the first mode shape.

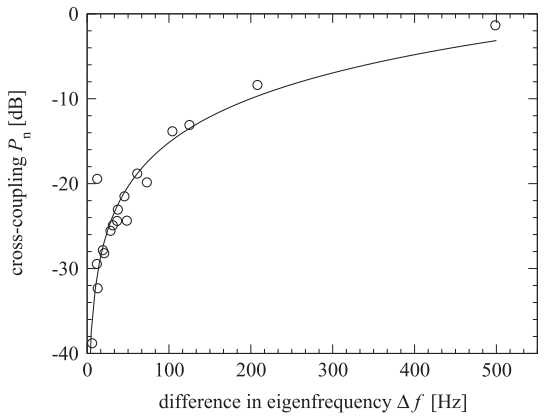

Fig. 6. Dependence of cross-coupling P_n on difference in eigenfrequency Δf between in-phase and out-of-phase mode.

3. Stop band material as backing

Mechanical cross-coupling in phased array transducers is highly influenced by the dynamic behavior of the backing as shown above. However, the reduction of cross-coupling by minimizing the difference in eigenfrequency between the in-phase and out-of-phase mode is connected to avoid the coincidence of backing dominating modes with the operating frequency. This leads to design issues for arrays with a larger number of transducer elements. More transducer elements require a larger backing. Thus, the modal density increases in the frequency range around the operating frequency. The matter even getting worse if the operating frequency is increased. To overcome this problem, a stop band material is introduced as a common backing. Stop band material can attenuate the wave propagation in the backing. Therefore, we create an extended model derived from the generic model. It contains a large number of small, equal resonators on the downside of the backing. These resonators can be tuned in

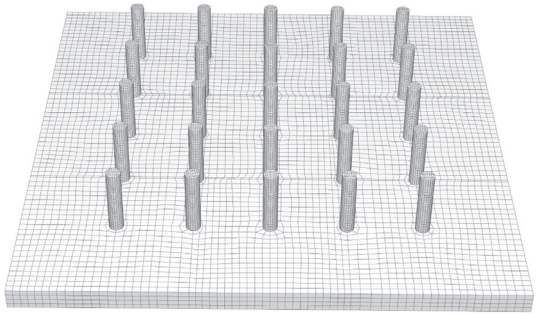

Fig. 7. Finite element model of the backing with a 5 × 5 grid of beam resonators on the downside.

order to change the frequency range where the backing shows a stop band behavior.

3.1. Design of stop band material

Stop band behavior in plates can be obtained if the resonator spacing s_{res} fits the requirement to be small enough in relation to the wavelength in the backing. Therefore, the ratio of the resonator frequency f_{res} to the frequency where the wavelength in the backing equals twice the resonator spacing $f_{\mathrm{plate}_{\lambda=2s_{\mathrm{res}}}}$ should be equal to or less than 1 [15]. According to Kirchoff plate theory, the wavelength in infinite plates is calculated by

$$\lambda = \frac{c_{\mathrm{plate}}}{f} \,, \tag{5}$$

with

$$c_{\mathrm{plate}} = \sqrt{\omega} \cdot \sqrt[4]{\frac{h^2\ E}{12\ \rho\ \left(1-\nu^2\right)}} \,.$$

A basic description is given in Ref. [28, p. 146].

Following the guideline given in Ref. [15] for the dimensionless frequency ratio

$$\frac{f_{\mathrm{res}}}{f_{\mathrm{plate}_{\lambda=2s_{\mathrm{res}}}}} \leq 1 \,, \tag{6}$$

the maximum resonator spacing s_{res} can be calculated by

$$f_{\mathrm{plate}} = \frac{2\pi}{\lambda^2}\sqrt{\frac{h^2\ E}{12\ \rho\ (1-\nu^2)}} \,, \tag{7}$$

$$s_{\mathrm{res}} = \sqrt{\frac{\pi\sqrt{\frac{h^2\ E}{12\ \rho\ (1-\nu^2)}}}{2f_{\mathrm{res}}}} \,. \tag{8}$$

The resonators will be tuned so that the first resonance frequency f_{res} coincides with the operating frequency of the bending elements of the phased array transducer $f_{\mathrm{r}} = 5.2$ kHz. The calculated wavelength is $\lambda = 44.5$ mm for the backing without resonators at this frequency. This result has been verified in a time domain simulation of the finite element model. Consequently, the resonator spacing should be less than 22.3 mm. To investigate the influence of stop band material on cross-coupling in the generic model, a 5 × 5 grid of beam resonators is used as shown in Fig. 7. In order to reduce cross-coupling, a significant wave attenuation between the bending elements is desired. Therefore, a spatial placement with one row of resonators between the bending elements is applied. The center to center spacing of the resonators is set to $s_{\mathrm{res}} = 10.75$ mm which corresponds to $s_{\mathrm{res}} \approx \lambda/4$. The resonators with a diameter of 2.05 mm can be tuned by trimming the beams length. The influence of stop band material on the cross-coupling is investigated for the system with $t_{\mathrm{b}} = 3$ mm. This system has high cross-coupling. In simulation, the beam resonators are modeled with C3D20R elements with a structured mesh. The average element edge length is 0.2 mm. The beam resonators are connected with a tie constraint by a surface-to-surface formulation to the backing. Studies show that the error introduced by meshing is negligible for the effect of cross-coupling.

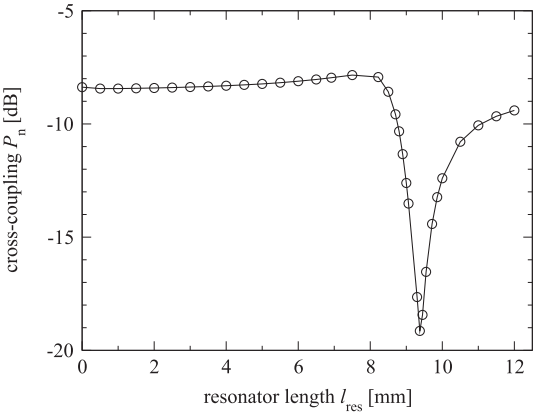

Fig. 8. Cross-coupling P_n dependence in the extended model on resonator length l_{res}.

3.2. Cross-coupling dependence on resonator length

The beam length is varied in a range between $1 \cdot 10^{-3}$ mm and 12 mm. Fig. 8 shows the cross-coupling dependence on the resonator length. Between 8.9 mm and 9.5 mm a high attenuation in cross-coupling can be achieved. In this range, the band of resonance frequency of the resonators fits the resonance frequency of the bending elements. The backing shows stop band behavior and the free wave propagation is attenuated. At a resonator length of 9.4 mm, the system has minimum cross-coupling with −19.1 dB.

In this configuration, the resonators increase the mass of the backing by 5.3% in comparison to the generic model without resonators. The influence of increased mass is evaluated in the generic model without resonators. Therefore, the density of the backing is increased by 5.3% in finite element simulation which leads to $P_n = -7.2$ dB. In this way, it is shown that the reduction of cross-coupling is not caused by the added mass but by the dynamic behavior of the stop band material.

3.3. Stop band behavior

Dispersion curves are common to analyze the behavior of periodic structures. The aim is to identify wave propagation in structures within a certain frequency range. In this study, they are calculated by applying the Floquet Bloch theorem in an undamped finite element model. The simulations are carried out with the commercial software COMSOL Multiphysics 5.3. As the theory of calculation is widely discussed in literature and is not on scope of this work, the authors refer to literature, e.g. Refs. [15,17,29,30].

The dispersion curves are used to proof the stop band behavior of the above described backing with attached beam resonators of the length 9.4 mm. As a reference, wave propagation is calculated for a unit cell representing the pure backing without a beam resonator as shown in Fig. 9 (a). The dimensions of the plate-like part of the unit cells are identical. The lattice has a 2D periodicity. Due to symmetry of the square unit cell, wave propagation has to be calculated along the contour of the triangle ΓXMΓ, cf. Fig. 9. The triangle represents the so called irreducible Brillouin zone (IBZ) [15].

To identify different types of waves propagating at the operating frequency of the phased array transducer, Fig. 10 shows the displaced unit cell of the pure backing. The corresponding points are marked in Fig. 11. Analyzing the displacements, three different wave types are found, an in-plane longitudinal wave ($\star$), a shear wave ($\circ$), and a bending wave ($*$). Comparable results with regard to a plate-like structure without resonators are described in Ref. [31]. Fig. 11 (b) shows the dispersion curves of the unit cell with an attached beam resonator. A major influence on the propagation of the shear wave and the bending wave is obtained. Thus, shear waves and bending waves can not propagate in the backing at the operating frequency of the phased array transducer. This reduces mechanical cross-coupling caused by a common backing.

To ensure that the stop band is related to the resonant behavior of the beam, dispersion curves of two additional test cases are calculated. The test cases refer to a beam length of 7.0 mm, cf. Fig. 12 (a) and 11.0 mm, cf. Fig. 12 (b). It is shown that changing the length of the beam resonator results in a changed stop band. Thus, the stop band with no wave propagation for shear and bending waves does not coincide with the operating frequency. In the first test case with beam length of 7.0 mm, in-plane longitudinal wave, shear wave, and bending wave can propagate at the operating frequency. In the second test case, the dispersion curves present at the operating frequency contain shear wave components. It is shown that the stop band is related to the resonant behavior of the beam. Due to the small width of the stop band, cf. Fig. 11, and the high sensitivity to the beam length, cf. Fig. 12, the curve of Fig. 8 shows high sharpness in the range between 8.0 mm and 11.0 mm. Finally, the reducing of mechanical cross-coupling can be admitted to the application of resonant stop band material as backing.

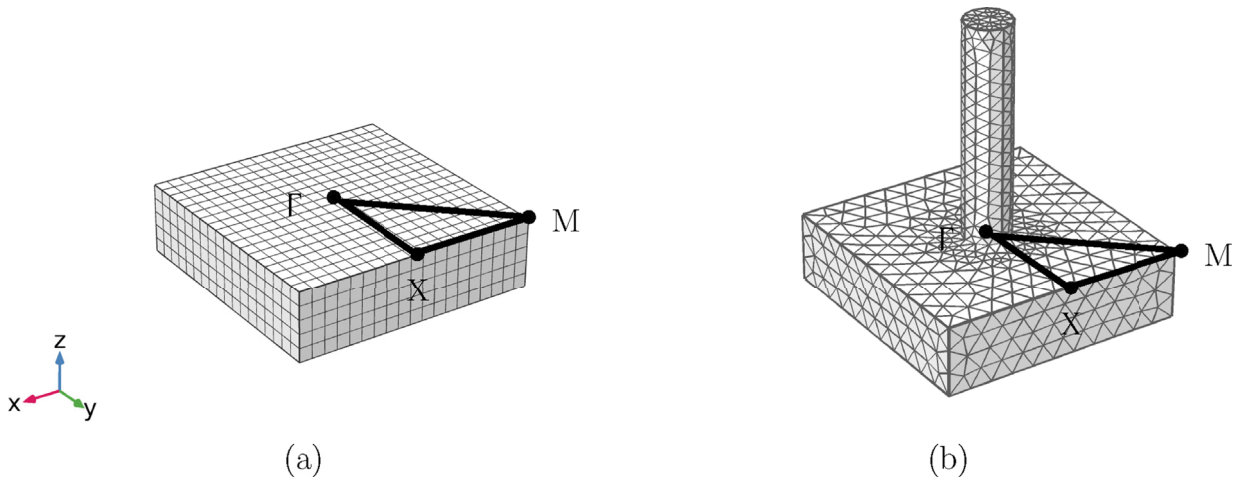

Fig. 9. (a) Unit cell without beam resonator. (b) Unit cell with attached beam resonator of 9.4 mm length.

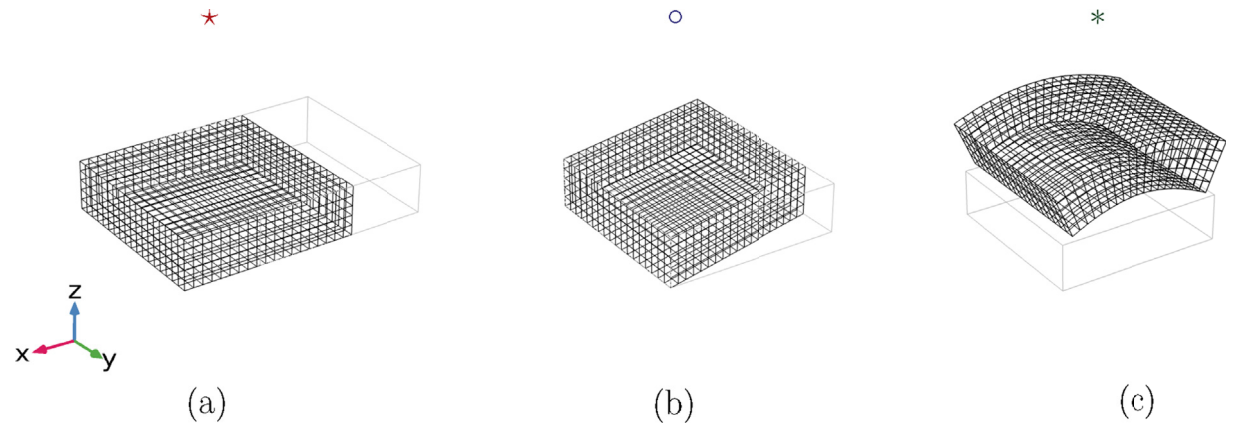

Fig. 10. The displacements of the unit cell without beam resonator are shown for the corresponding points marked in Fig. 11 (a). Three different wave types are identified: in-plane longitudinal wave (a), the shear wave (b), and the bending wave (c). The undeformed outlines are shown in gray.

4. Experimental validation

In this section, we validate the finite element simulation for the generic model as well as for the extended model by experimental testing. Firstly, we describe the specimen preparation and test setup. Afterwards, the effect of stop band materials on cross-coupling in a real setup is shown and compared to the results from Section 3. Finally, we compare the frequency response function (FRF) from the finite element simulation and the experiment to evaluate the differences between numerical and experimental results.

4.1. Specimen preparation and assembling

The experimental validation requires specimens with high geometrical accuracy. A major challenge is the preparation of an epoxy backing with 25 local resonators. The preparation as one piece is desired to avoid additional joints between backing and resonators which may have different mechanical properties. The preparation of the backing with local resonators can be done by casting epoxy in a mold which has the negative form of the backing. Especially the demold process requires high effort since small and long resonator beams tend to break during demolding. This issue possibly increases in real world applications where the operating frequency is higher and consequently the dimensions of the stop band material are smaller. To overcome this issue, it would be possible to assemble separately manufactured beam resonators and backing in an additional process. Fig. 13 (a) shows the prepared backing with 25 beam resonator on the downside. The bending elements and the backing are coated with aluminum by thermal evaporation to form electrodes. By covering certain areas of the backing, it is possible to separate the counter-electrodes for each transducer element.

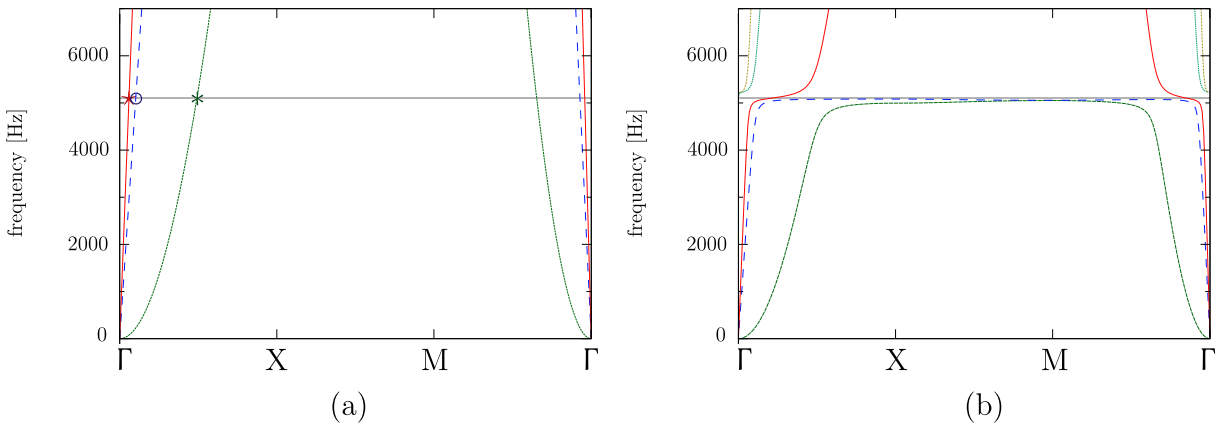

Fig. 11. Dispersion curves for different unit cells, operating frequency marked by horizontal line at 5.1 kHz (a) without beam resonator. (b) backing with attached, well tuned beam resonator, length 9.38 mm.

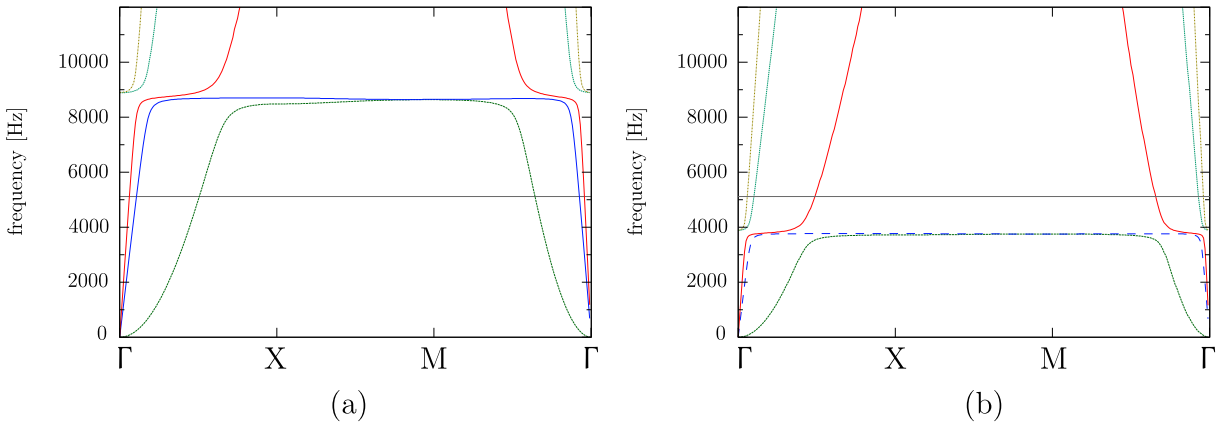

Fig. 12. Dispersion curves for different unit cells, operating frequency marked by horizontal line at 5.1 kHz (a) backing with attached, poorly tuned beam resonator, length 7.0 mm (b) backing with attached, poorly tuned beam resonator, length 11.0 mm.

Another challenging process is the assembling of the bending elements and the backing. The boundary conditions for the vibrational properties of the bending elements are defined by the length between the epoxy sockets. The bending elements are jointed with cyanoacrylate adhesive to the epoxy sockets. Thus, a small air gap between the electrodes is realized. The assembly is finished by connecting electrical wires with copper tape to the electrodes.

The influence of the local resonators on the cross-coupling is investigated with one and the same specimen. By this, differences in cross-coupling maybe caused by the single parts, preparation and assembly of the specimen can be avoided. The model is prepared using a backing with local resonators of 12 mm length. The length of the local resonators can be trimmed stepwise by sanding. In this way, it is possible to measure the cross-coupling influenced by local resonators with different length at one specimen.

4.2. Test setup for cross-coupling measurement

For experimental testing of cross-coupling, a non-contact measurement is done with a scanning laser Doppler vibrometer. The specimen is placed on two horizontal tighten yarns. By this, free-free boundary conditions can be approximated. Fig. 13 (b) shows the set up generic model during experimental testing. The active element is excited by an electrical voltage between the capacitor electrodes. In a range from 4.5 kHz to 6 kHz a periodic signal, called pseudo random, is applied. This signal type excites all frequencies of the measured spectrum simultaneously and does not cause leakage effects [32]. The signal from the signal generator is amplified with a high voltage amplifier which amplifies the alternating current (AC) excitation voltage and

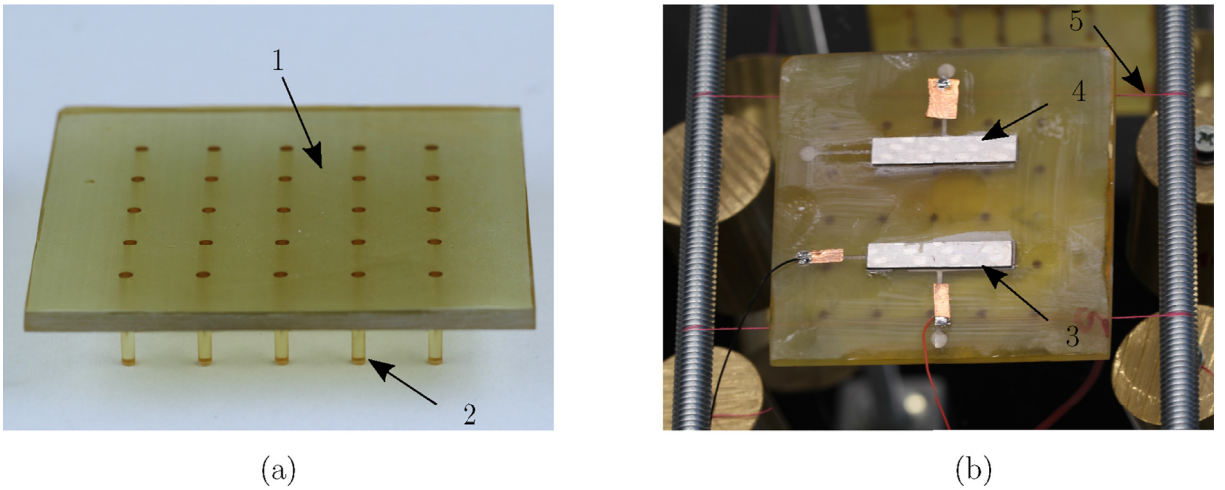

Fig. 13. Backing with beam resonators (a) and experimental test setup (b): (1) backing, (2) beam resonator, (3) active bending element, (4) passive bending element, (5) tighten yarn.

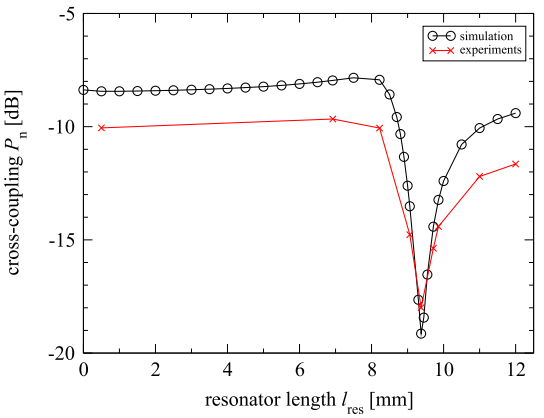

Fig. 14. Cross-coupling P_n dependence on resonator length l_{res} in the extended model. Comparison of results from simulations and experiments.

generates an additional 200 V direct current (DC) offset. The velocity spectrum is measured at 27 scanning points for each bending element. Cross-coupling is calculated at the resonance frequency of each bending element like described in Eq. (4).

4.3. Cross-coupling dependence on resonator length

The length of the beam resonators is trimmed to fit the stop band to the operating frequency of the phased array transducer. Fig. 14 shows the cross-coupling depending on the resonator length. Between 9.0 mm and 10 mm, a major reduction of cross-coupling is achieved in simulation as well as in experiment. Reasonable agreement between numerical simulation and experimental testing is attained. The reduction in cross-coupling is attributed to the stop band behavior of the backing achieved by the local resonators on the downside. The most effective reduction can be achieved at 9.4 mm. The mechanical cross-coupling is reduced from −10.1 dB to −18.0 dB.

In case of resonators with 12 mm length, the frequency range of the stop band does not coincide with the operating frequency of the phased array transducer. The mechanical cross-coupling is −11.6 dB. By this, it is verified that the reduction of cross-coupling is caused by the stop band behavior.

4.4. Harmonic analysis

To evaluate the differences between simulation and experiment, the FRFs of both are compared. Therefore, the generic model without resonators and $t_b = 3$ mm is analyzed. As the electrodynamic behavior is out of scope of this study, the excitation in the finite element simulation is applied by a mechanical load. However, the input parameter for the experiment is an electrical

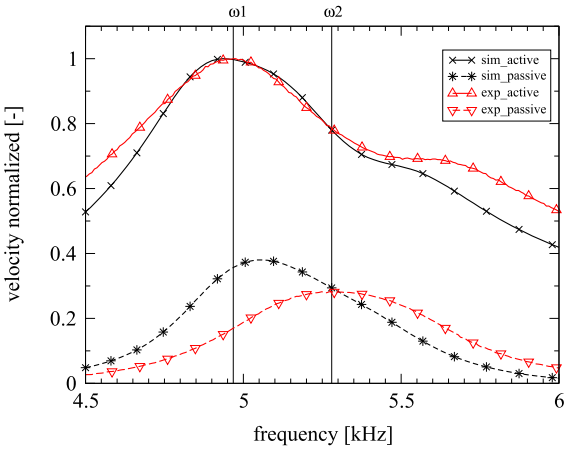

Fig. 15. Normalized frequency spectrum from simulation and experimental testing of the generic model. Results from numerical simulation active (×) and passive (∗) bending element. Results form experimental testing (△) and passive (▽) bending elements.

voltage. To compare the FRFs of the experiment and simulation, they are normalized to 1 at maximum of the active bending element. Fig. 15 shows a reasonable agreement between simulation and experiment.

In the experiment, a shift in resonance frequency for the passive bending occurs. This can be ascribed to small differences in free length of the bending element. Due to the rheological behavior, the adhesive easily flows and changes free length between the epoxy sockets in preparation process. As the resonance frequency is highly sensitive to the free length, this is a major challenge during the application process of the bending elements. In Section 2, the calculation of cross-coupling P_{n} is explained. Analyzing Fig. 15 it becomes clear, that it leads to differences whether P_n is calculated at a fixed frequency by $P_{\mathrm{n}} = \frac{V_2(\omega 1)}{V_1(\omega 1)}$, e.g. the resonance frequency of the active element, or at the resonance frequency of each bending element $P_{\mathrm{n}} = \frac{V_2(\omega 2)}{V_1(\omega 1)}$.

4.5. Discussion

The simulations of the generic and the extended models are validated with experimental measurements. In configurations with resonator length 1 mm–9 mm and 10 mm–12 mm, the frequency range of the stop band is poorly tuned to the operating frequency. In this cases, less cross-coupling is present in experiments than in simulations. This can be attributed to different resonance frequencies of the bending elements in experiments. Furthermore, cross-coupling is highly influenced by damping. As the precise determination of dynamic material parameters, given in Table 2, is complex and influenced by uncertainties, this can be another reason for this differences. However, the accordance between simulation and experimental measurements is quite good as the absolute difference in cross-coupling P_{n} varies between 1.3 dB and 2.2 dB. The frequency range of the stop band and the operating frequency coincides between 9 mm and 10 mm resonator length. In this case, a major reduction of cross-coupling is obtained in simulations and in experiments. It is reduced in experiments by 7.9 dB. In contrary to the poorly tuned configuration, the cross-coupling at 9.4 mm is higher in the experiment than in simulation. The reason for that can be found in tuning the resonators by sanding. This causes a variance in the length of each resonator. Thus, the effect of wave attenuation at a certain frequency is smaller than under ideal conditions, where the resonators have all the same length. Nevertheless, the difference between the simulation and the experimental measurements is only 1.1 dB.

5. Conclusion

The authors presented a study on mechanical cross-coupling in air-coupled phased array transducers with low operating frequency. In a generic model, the behavior of cross-coupling is investigated with special focus on the influence of the common backing. In finite element simulation, a generic model with two single transducers is set up. They are realized as capacitive transducers with bending elements which are bonded on the common backing. In order to reduce mechanical cross-coupling, stop band material as backing is investigated in this study. Therefore, beam resonators are attached on the downside of the backing. The frequency range of the stop band is tuned by trimming the length of the beam resonators. The effect on cross-coupling is investigated in numerical simulation and experimental testing. The authors conclude that in low frequency air-coupled phased array transducers

(i) mechanical cross-coupling highly depends on the particular dynamic behavior of the common backing,
(ii) the difference in eigenfrequency between in-phase and out-of-phase mode of the bending elements is an indicator of mechanical cross-coupling. A higher difference in eigenfrequency indicates a stronger mechanical cross-coupling and

(iii) stop band material realized with local resonators on the downside of the backing is a suitable solution to achieve a major reduction of mechanical cross-coupling.

The presented results offer a new possibility to estimate mechanical cross-coupling in similar low frequency phased array transducers with a common backing based on a modal analysis. This is an advantage for optimization problems, as a modal analysis usually requires less computational effort than a harmonic analysis. In further studies, the influence of uncertainties in material and geometry should be investigated in detail. Nevertheless, by experimental results of this study it is shown that a major reduction in mechanical cross-coupling can be achieved with stop band material in a real setup.

Acknowledgements

The authors gratefully acknowledge Robert Bosch GmbH Germany for the funding of this research.

References

[1] S. Harput, A. Bozkurt, F.Y. Yamaner, Ultrasonic phased array device for real-time acoustic imaging in air, in: IEEE Ultrason. Symp, 2008, pp. 619–622.
[2] S. Harput, A. Bozkurt, Ultrasonic phased array device for acoustic imaging in air, IEEE Sens. J. 8 (11) (2008) 1755–1762.
[3] G.S. Kino, Acoustic imaging for nondestructive evaluation, Proc. IEEE 67 (4) (1979) 510–525.
[4] D. Ekeom, A.H. Henni, G. Cloutier, Design of a phased-array for radiation force generation following a closed path, in: IEEE Int. Ultrason. Symp, 2010, pp. 662–665.
[5] R.L. Baer, G.S. Kino, Theory for cross coupling in ultrasonic transducer arrays, Appl. Phys. Lett. 44 (10) (1984) 954–956.
[6] J.D. Larson, Non-ideal radiators in phased array transducers, in: Ultrason. Symp, 1981, pp. 673–684.
[7] J. Dias, An experimental investigation of the cross-coupling between elements of an acoustic imaging array transducer, Ultrason. Imaging 4 (1) (1982) 44–55.
[8] C. DeSilets, Transducer Arrays Suitable for Acoustic Imaging, Ph.D. thesis, Stanford Univ., CA, 1978.
[9] J.S. Bird, S. Asadov, P. Kraeutner, Improving arrays for multi-angle swath bathymetry, in: Oceans Conference Record (IEEE), vol. 4, 2003, pp. 2085–2092.
[10] A. Bozkurt, F.L. Degertekin, A. Atalar, B.T. Khuri-Yakub, Analytic modeling of loss and cross-coupling in capacitive micromachined ultrasonic transducers, in: IEEE Ultrason. Symp., vol. 2, 1998, pp. 1025–1028.
[11] R.J. Kazys, R. Sliteris, J. Sestoke, Air-coupled low frequency ultrasonic transducers and arrays with PMN-32% PT piezoelectric crystals, Sensors 17 (2017) 1–20.
[12] M. Celmer, K. Opielinski, Research and modeling of mechanical crosstalk in linear arrays of ultrasonic transducers, Arch. Acoust. Q. 41 (3) (2016) 599–612.
[13] M. Celmer, K.J. Opielinski, M. Dopierala, Structural model of standard ultrasonic transducer array developed for fem analysis of mechanical crosstalk, Ultrasonics 83 (2018) 114–119.
[14] Z. Liu, X. Zhang, Y. Mao, Y.Y. Zhu, Z. Yang, C.T. Chan, P. Sheng, Locally resonant sonic materials, Science 289 (5485) (2000) 1734–1736.
[15] C.C. Claeys, K. Vergote, P. Sas, W. Desmet, On the potential of tuned resonators to obtain low-frequency vibrational stop bands in periodic panels, J. Sound Vib. 332 (2013) 1418–1436.
[16] C.C. Claeys, P. Sas, W. Desmet, On the acoustic radiation efficiency of local resonance based stop band materials, J. Sound Vib. 333 (2014) 3203–3213.
[17] C. Kittel, Introduction to Solid State Physics, Wiley, Hoboken, NJ, 2005.
[18] N. Kaina, F. Lemoult, M. Fink, G. Lerosey, Ultra small mode volume defect cavities in spatially ordered and disordered metamaterials, Appl. Phys. Lett. 102 (14) (2013) 144104.
[19] M. Rupin, F. Lemoult, G. Lerosey, P. Roux, Experimental demonstration of ordered and disordered multiresonant metamaterials for lamb waves, Phys. Rev. Lett. 112 (2014) 234301.
[20] Y. Xiao, J. Wen, X. Wen, Flexural wave band gaps in locally resonant thin plates with periodically attached spring-mass resonators, J. Phys. D Appl. Phys. 45 (19) (2012) 195401.
[21] R.H. Olsson III, I. El-Kady, Microfabricated phononic crystal devices and applications, Meas. Sci. Technol. 20 (1) (2009) 012002.
[22] S. Köllner, Modelling and Simulation of Ultrasonic Transducers Based on Composites (Modellbildung und Simulation von Ultraschallwandlern auf Basis von Verbundwerkstoffen), Karlsruhe Institute of Technology, Department of Mechanical Engineering, 2014. Master's thesis.
[23] J.C. Halpin, J.L. Kardos, The halpin-tsai equations: a review, Polym. Eng. Sci. 16 (5) (1976) 344–352.
[24] D. Hull, T.W. Clyne, An Introduction to Composite Materials, second ed., Cambridge Solid State Science Series, Cambridge University Press, 1996.
[25] R. Akkerman, Laminate mechanics for balanced woven fabrics, Compos. B Eng. 37 (2) (2005) 108–116.
[26] P. Langer, M. Maeder, C. Guist, M. Krause, S. Marburg, More than six elements per wavelength: the practical use of structural finite element models and their accuracy in comparison with experimental results, J. Comput. Acoust. 25 (4) (2017) 1750025.
[27] R. Reiß, Simulation and Optimization of Ultrasonic Transducers in Arrays (Simulation und Optimierung von Ultraschallwandlern im Mehrelemente-Verbund), University of Stuttgart, Institute of Applied and Experimental Mechanics, 2014. Master's thesis.
[28] M. Möser, Technical Acoustics (Technische Akustik), tenth ed., Springer-Verlag, Berlin Heidelberg New York, 2015.
[29] L. Brillouin, Wave Propagation in Periodic Structures: Electric Filters and Crystal Lattices, Dover Publications, 1953.
[30] M. Collet, M. Ouisse, M. Ruzzene, M. Ichchou, Floquet–bloch decomposition for the computation of dispersion of two-dimensional periodic, damped mechanical systems, Int. J. Solids Struct. 48 (20) (2011) 2837–2848.
[31] C. Claeys, E. Deckers, B. Pluymers, W. Desmet, A lightweight vibro-acoustic metamaterial demonstrator: numerical and experimental investigation, Mech. Syst. Sig. Process 70 (2016) 853–880.
[32] Polytec GmbH, Polytec-Platz 1-7, 76337 Waldbronn, Germany, Theory Manual Polytec Scanning Vibrometer PSV Theory, As of Software 9.1 Edition.